THE JOURNAL OF PHYSICAL CHEMISTRY B

B: Fluid Interfaces, Colloids, Polymers, Soft Matter, Surfactants, and Glassy Materials

Molecular Dynamics Simulation of Interaction between Functionalized Nanoparticles with Lipid Membranes: Analysis of Coarse-Grained Models

Mitradip Das, Udaya Dahal, Oluwaseun Mesele, Dongyue Liang, and Qiang Cui

J. Phys. Chem. B, **Just Accepted Manuscript** • DOI: 10.1021/acs.jpcb.9b08259 • Publication Date (Web): 01 Nov 2019

Molecular Dynamics Simulation of Interaction between Functionalized Nanoparticles with Lipid Membranes: Analysis of Coarse-grained Models

Mitradip Das,[†,‡,⊥] Udaya Dahal,[¶,⊥] Oluwaseun Mesele,[¶] Dongyue Liang,[§] and Qiang Cui[*,‖]

†*Integrated MSc, School of Chemical Sciences, National Institute of Science Education and Research, Khordha, Odisha, India, 752050*

‡*Homi Bhabha National Institute, Training School Complex, Anushaktinagar, Mumbai, Maharashtra, India, 400094*

¶*Department of Chemistry, Boston University, 590 Commonwealth Avenue Boston, MA 02215*

§*Department of Chemistry and Theoretical Chemistry Institute, University of Wisconsin-Madison, 1101 University Avenue, Madison, WI 53706*

‖*Departments of Chemistry, Physics and Biomedical Engineering, Boston University, 590 Commonwealth Avenue Boston, MA 02215*

⊥*Contributed equally to this work*

E-mail: qiangcui@bu.edu, Tel:(+1)-617-353-6189

Abstract

We compare atomistic and two popular coarse-grained (POL- and BMW-MARTINI) models by studying the interaction between a cationic gold nanoparticle functionalized with primary alkane amines and a lipid bilayer that consists of either zwitterionic lipids or a mixture of zwitterionic and anionic lipids. In the atomistic simulations, the nanoparticle does not exhibit any notable affinity to the zwitterionic bilayer but readily binds to the 9:1 zwitterionic:anionic bilayer, and nanoparticle adsorption leads to local segregation of anionic lipids and slowing down of their diffusion. At the coarse-grained level, the POL-MARTINI model does not lead to nanoparticle-membrane binding for either bilayer systems, while the BMW-MARTINI model leads to nanoparticle binding to both bilayers; with the BMW-MARTINI model, nanoparticle binding leads to much less demixing of zwitterionic and anionic lipids and moderately *higher* rates of lipid diffusion. Analysis of nanoparticle properties in solution reveals notable discrepancies in the interfacial charge and water distributions at the coarse-grained level that are likely relevant to their limitations in describing binding interactions with other (bio)molecules.

1 Introduction

There is an increasing interest in understanding at the molecular level how nanomaterials interact with biological systems such as proteins and lipid membranes.[1–6] Such mechanistic studies will be able to inform the design of new nanomaterials for better functionality (e.g., drug discovery) and less negative environmental and health impact. Due to the complexity and heterogeneity of nanomaterials, probing the nano/bio interface at the molecular level requires the integration of multiple experimental approaches[4,7–11] as well as computational analyses.[12–14] For the latter, in addition to atomistic studies at quantum and classical levels,[15–17] coarse-grained models are also important as many processes at the nano/bio interface involve rather large length and temporal scales and therefore beyond the reach of atomistic simulations. In the past decades, different coarse-grained models such as MARTINI,[18–21] Dissipative Particle Dynamics[22,23] and continuum mechanics models[24–28] have been used to probe the interaction between nanoparticles with proteins and lipid membranes. Interesting mechanistic insights have been gleaned from these studies, such as the roles of shape, orientation and surface composition of nanoparticles (e.g., protein corona[29]) in determining their interaction with membrane and cellular uptake.[24,27,30,31]

An important and general challenge to coarse-grained simulations is to establish that the model is sufficiently reliable for probing the questions of interest for the system in hand. Since most coarse-grained models were developed based on a selected set of observables, it is often not clear whether they are readily transferrable to the specific system of interest. For example, the MARTINI set of models,[32,33] which has been tremendously successful for studying lipid systems,[18,34] were developed based largely on thermodynamic quantities (transfer free energies of molecules from water to non-polar liquids) and selected structural properties (e.g., area per lipid), thus it is not readily clear how transferable the parameters are for modeling processes at the nano/bio interface. Many functionalized nanoparticles feature surface charge densities substantially higher than a typical protein,[35] therefore treating electrostatic interactions in a reliable fashion is likely essential. Indeed, in a recent study,[36] Sheavly

et al. found that three different parameterizations of the MARTINI model (MARTINI,[32] POL-MARTINI[37] and BMW-MARTINI[38,39]) led to drastically different potentials of mean force for the binding of a cationic nanoparticle to a zwitterionic (phosphatidylcholine) multi-component lipid bilayer (dilinoleoyl phosphatidylcholine + dipalmitoyl phosphatidylcholine + cholesterol); MARTINI led to a very weak binding of 3-5 k_BT, BMW-MARTINI led to substantially stronger binding of ∼30-50 k_BT to different phases (liquid ordered vs. liquid disordered) of the bilayer, while POL-MARTINI led to a purely repulsive interaction. Since the BMW-MARTINI model gives an interfacial electrostatic potential profile that most resembles the atomistic result,[38,39] it was concluded that the BMW-MARTINI results were most reliable; this was also indirectly supported by the qualitative agreement with experimental measurements of binding for the similar systems.[40] Nevertheless, a more explicit comparison to atomistic simulation would have been valuable.

In this study, we compare atomistic and coarse-grained simulations of a gold nanoparticle functionalized by alkyl amines in both aqueous solution and at the surface of lipid bilayers; for the latter, we study a pure zwitterionic lipid bilayer and a two-component bilayer that consists of zwitterionic and anionic lipid molecules, since anionic lipids are common in cellular membranes.[41] We examine a fairly broad set of observables that include surface ligand orientation, ion and charge distributions around the nanoparticle, binding of the nanoparticle to lipid bilayers, and perturbations in lipid properties due to nanoparticle adsorption. With this fairly comprehensive set of comparisons, we conclude that the BMW-MARTINI model indeed appears more reliable than the POL-MARTINI model for probing nanoparticle/membrane interactions, although it also has several limitations that highlight the challenge of developing coarse-grained models for interfaces. The study underscores the importance of systematic calibration of popular coarse-grained models for probing complex systems and cautions the interpretation of coarse-grained simulations in the absence of atomistic or experimental data.

In the following, we first summarize the computational models and methodological de-

tails. We then present the comparison between atomistic and two popular coarse-grained (POL-MARTINI and BMW-MARTIN) models for the behaviors of the functionalized gold nanoparticle in aqueous solution and at the membrane/water interface. We end with several concluding remarks.

2 Computational Models and Methods

2.1 Atomistic Simulations

The gold nanoparticle studied here is of spherical shape and has a diameter of approximately 2 nm; it contains 240 gold atoms and is functionalized with 72 butyl amine ligands through thiol linkage. In our previous work,[35] we showed using a hybrid Monte Carlo/Molecular Dynamics scheme that with such ligand density ($\sim$3 molecules/nm^2), approximately half of the amines are expected to be protonated at neutral pH. Therefore, 38 amines are chosen to be positively charged, while the rest (34) is taken to be charge neutral; following this population ratio, amines are selected to be protonated at random. The nanoparticle is then solvated either in a water box (Fig. 1a) or placed on top (20 Å) of a lipid bilayer (Fig. 1b-c). Two bilayer systems are studied: one contains pure DMPC (1,2-dimyristoyl-sn-glycero-3-phosphocholine) while the other one is a mixture of DMPC and DMPG (1,2-dimyristoyl-sn-glycero-3-phospho-(1'-rac-glycerol)) with a ratio of 9:1. The equilibrated simulation box dimensions for the systems shown in Fig. 1a-c are approximately 10 $\times$10 $\times$ 10 nm^3 and 7 $\times$ 7 $\times$ 17 nm^3 for the aqueous solution and membrane setups, respectively. In all simulations, neutralizing ions were added and then a concentration of 0.15 M of NaCl is maintained, which is close to the physiological salt concentration.

The systems are generated using CHARMM-GUI[42,43] and simulated using NAMD.[44] For simulation of lipid bilayer systems, the CHARMM36m force field[45,46] is used while a different and partially customized force field[15] is used for the gold nanoparticle based on the INTERFACE force field;[47] water is treated with a modified TIP3P.[48,49] Temperature

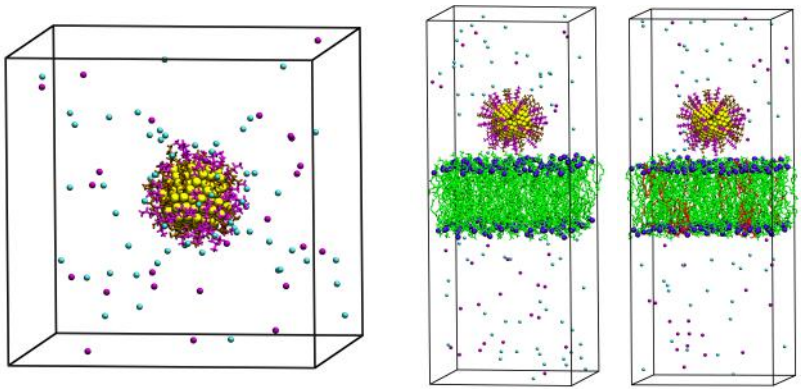

(a) (b) (c)

Figure 1: Snapshots for the initial configurations of atomistic simulations. (a) A gold nanoparticle with a diameter of 2 nm functionalized with 72 butyl amines (38 charged and 34 neutral) in a cubic water box of $\sim$ 10 nm in length and 150 mM NaCl; (b) The same gold nanoparticle placed at the surface of a bilayer that contains $\sim$180 DMPC lipids; (c) The same gold nanoparticle placed at the surface of a 9:1 DMPC:DMPG bilayer that contains $\sim$180 lipids in total. The DMPG and DMPC lipids are shown in green and red, respectively. Water molecules are excluded for clarity. The equilibrated simulation box dimension for the membrane systems is approximately $7 \times 7 \times 17$ nm^3.

is controlled using the Nose-Hoover thermostat,[50,51] and pressure is controlled with the Parrinello-Rahman barostat.[52] SHAKE[53] is used to constrain all bonds involving hydrogen, allowing an integration time step of 2 fs. Electrostatic interactions are treated using particle-mesh-Ewald[54] with a grid of 1 Å, and van der Waals interactions are treated using a switching function[55] between 10 and 12 Å. All simulations are equilibrated for a few nanoseconds before at least 100 nanoseconds of production run.

2.2 Coarse-grained Simulations

For the coarse-grained simulations, the same set of systems are studied with the POL-MARTINI[33,37] and BMW-MARTINI[38,39] models (see Fig. 2). We note that we have not included results for the standard MARTINI model[32] because water in such simulations is observed to have a high tendency to crystalize, even in the presence of a typical fraction ($\sim$10%) of anti-freezing particles. As discussed in the BMW-MARTINI studies,[38,39] this is likely a limitation of the standard MARTINI model for systems that feature a high amount

of charges.

For the nanoparticle, to be consistent with the atomistic model, a 2 nm diameter gold particle with 72 alkyl amine ligands (38 cationic + 34 neutral) is studied. The gold beads are treated as the P4 type and each alkyl amine ligand is treated with two coarse-grained beads; one bead is hydrophobic (C1), while the other is Q_d but with charge of either 0 or +1, depending on whether the amine is charge neutral or cationic. Simulations are also conducted in which the charge-neutral amine bead is treated as N_d, or all amine beads are of type Q_0, which mimics quaternary amines; the corresponding results are included in the **Supporting Information**.

Temperature is maintained at 300 K using the Berendsen thermostat[56] with a coupling time constant of 1 ps and the pressure is maintained at 1 bar using the Berendsen barostat;[56] the pressure coupling is semi-isotropic with coupling constant of 2 ps and compressibility of 3×10^{-5} bar^{-1}. Electrostatic interaction is calculated using the the particle-mesh-Ewald[54] and van der Waals interactions are treated using a switching function. Each simulation is carried out for at least 1 μs with an integration time step of 20 femtoseconds. For the POL-MARTINI lipid simulation, the dimension of the box is approximately 10nm $\times$ 10nm $\times$ 14nm, while for the BMW-MARTINI lipid simulations, to test the finite size effect, the simulation box is taken to be larger in the x direction and has the dimension of approximately 20 $nm \times 10\ nm \times 13\ nm$. For the solution systems, the system box is a cube of approximately 12 nm in length with both models. All coarse-grained simulations are carried out using GROMACS gpu version 2016.3.[57]

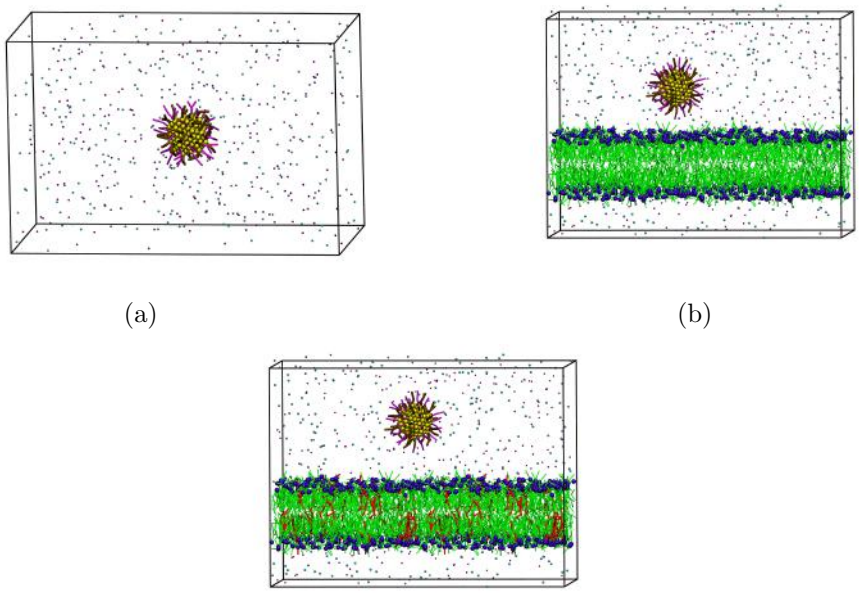

(a) (b)

(c)

Figure 2: Same as Fig. 1, but for snapshots for the initial configurations of the BMW-MARTINI simulations. The color schemes for the nanoparticle and lipids are consistent with those for the atomistic models shown in Fig. 1.

3 Results and Discussion

3.1 Functionalized Nanoparticle in water

3.1.1 Ligand Configurations

For a nanoparticle in water, the charged amine ligand mainly points to solution, as indicated by the relatively narrow single peak for the radial distribution function of nitrogen relative to the nanoparticle center (Fig. 3a). For the neutral ligand, the nitrogen radial distribution function exhibits two peaks (Fig. 3b), indicating two dominant orientations: the peak at the longer distance resembles that for the cationic ligand, indicating the similar ligand orientation pointing into solution; the peak at the shorter distance corresponds to an orientation where the ligand lies closer to the nanoparticle surface (see Fig. 3c for an illustration). The two orientations are similar to those observed for alkyl amines at the gold (100)/water interface in our previous study,[15] in which the finding was validated by comparing full QM (DFT and CCSD(T)), QM/MM free energy path[58,59] and MM simulations; in essence, the neutral amine group has a higher tendency to lie close to the gold atoms compared to the cationic amine group due to the smaller desolvation penalty.

It is encouraging that qualitatively similar trends are observed at the coarse-grained level. As shown in Fig. 3a-b for the BMW-MARTINI simulation, the radial distribution functions of "amine nitrogen" relative to the center of the nanoparticle also exhibit different numbers of peaks, depending on the charge state of the amine group. At the coarse-grained level, however, the neutral ligand has a higher probability density for the orientation in which the amine group remains close to the gold surface (Fig. 3d).

3.1.2 Ion and Charge Distributions around the Nanoparticle

Since counter ions play a major role in modulating the electrostatic properties of charged nanoparticles,[60] we next analyze the ion and charge distributions around the nanoparticle. For the cationic amine, the radial distribution function of Cl^- around the amine nitrogen

(Fig. 4a) is dominated by a large peak at short distance (∼3.2 Å), reflecting strong first-shell coordination of Cl^- with NH_3^+; a minor peak at ∼5.5Å reflects the weaker second-shell coordination. For the neutral amine ligands (Fig. 4b), the Cl^- association is substantially weaker, as reflected by the much smaller peak values; the presence of multiple peaks reflect, in part, the fact that neutral amine ligands have multiple surface orientations as discussed above. The charge density and its molecular components are shown in Fig. 5a; the rapid oscillation of the charge density around zero is a result of charge compensation between the ligand amine groups, salt ions as well as interfacial water molecules. For example, the oscillation near the nanoparticle surface ($10 \leq r \leq 13$ Å) is largely due to the interplay between the neutral amine ligands and water, while contributions from charged amine groups and Cl^- start to dominant only at larger distances ($r > 13 - 15$ Å) due to the fact most charged amines prefer well solvated and thus remain further from the particle surface.

At the coarse-grained level, for both BMW- and POL-MARTINI, the Cl^- radial distribution functions around the "amine" groups show qualitatively similar behaviors: for the cationic amine group, the distribution function has a single dominant peak, followed by a substantially lower second peak (Fig. 4a); for the neutral amine group, the distribution function features multiple peaks with lower values (Fig. 4b), as expected from the multiple orientations of the neutral ligands and weaker association with Cl^- ions. Due to the coarse-grained nature of the amine group, however, the peak heights and locations in the radial distribution functions do not match the atomistic results quantitatively, as expected from the lack of multiple polar hydrogens in the amine group at the coarse-grained level, and the fact that a coarse-grained Cl^- better mimics a chloride ion with a first solvation shell. Comparing BMW- and POL-MARTINI models, it seems that Cl^- has a higher affinity to the amine beads, irrespective of charge, at the BMW-MARTINI level compared to the POL-MARTINI model; this is reflected by the systematically higher peaks in the RDFs at the BMW-MARTINI level, and the difference is more dramatic for the case of neutral amine, for which the height for the first peak is ∼11 and ∼2 with BMW- and POL-MARTINI,

respectively, in comparison to the value of ∼6 at the all-atom level (Fig. 4b).

For the charge density profile (Fig. 5b-c), especially with the BMW-MARTINI model, the qualitative trends resemble those found for the atomistic simulations (Fig. 5a): there are oscillations around zero due to compensation between the charged ligands, salt ions and interfacial water. At the quantitative level, however, the magnitude of oscillation with the BMW-MARTINI model is somewhat larger and also persists to a longer range ($r \sim 25$ Å vs. $r \sim 17$ Å). Moreover, although the neutral amine does not bear any charge at the coarse-grained level (the atomistic model still has partial charges for the atoms in the neutral amine) and therefore do not contribute directly to interfacial charge density, they do influence the orientation of water molecules close to the nanoparticle. As a result, the charge density with BMW-MARTINI features a positive peak at short distance ($r \sim 13$ Å) due entirely to the charges in the coarse-grained water "molecules", while a peak in the all-atom model at this distance is due to the neutral amine ligands with little contribution from water; by contrast, POL-MARTINI does not feature any obvious peak at distance below 15 Å, suggesting much weaker water-ligand interactions. For the Cl^- contribution to charge density, BMW-MARTINI features a notable peak at short (∼13 Å) distance and small but non-negligible contributions up to 25 Å, while the POL-MARTINI model leads to very minor Cl^- contribution at all distances; this difference is consistent with the substantially weaker Cl^--amine association at the POL-MARTINI level as reflected by the radial distribution functions discussed above. Overall, the BMW-MARTINI model leads to a better agreement in the interfacial charge density distribution with all-atom result than POL-MARTINI, hinting at a more reliable coarse-grained description of nanoparticle binding to other biomolecules, such as a lipid bilayer.

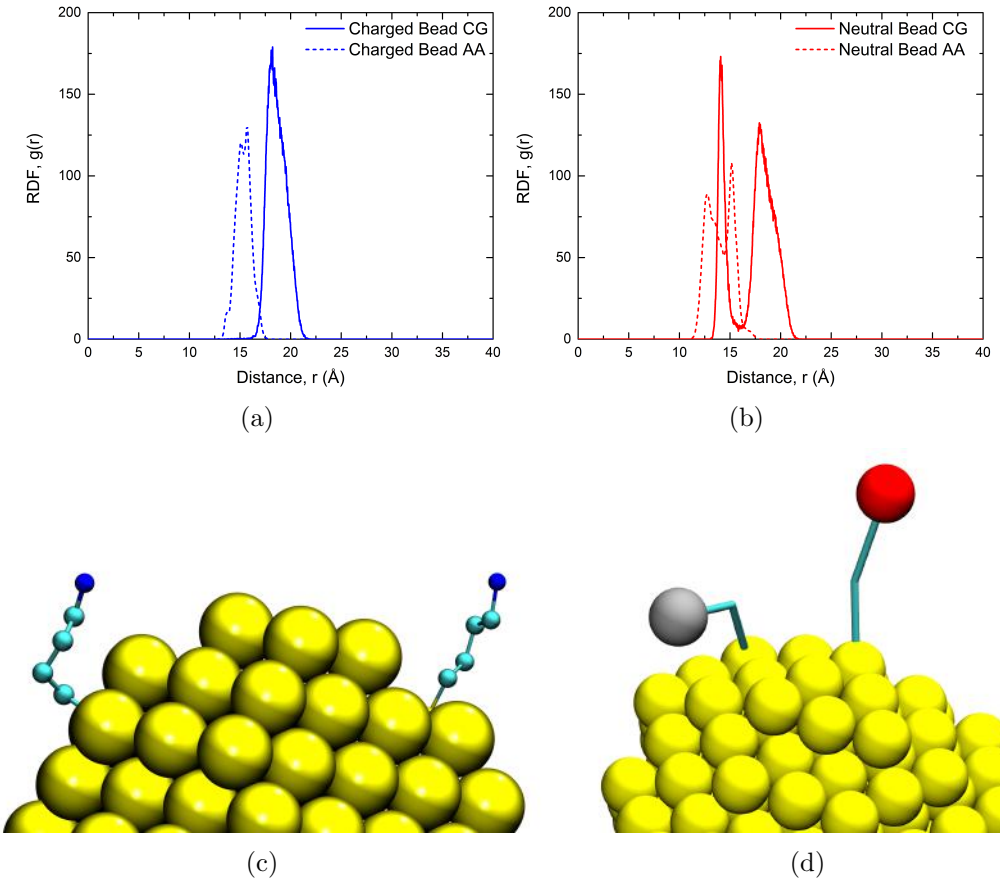

Figure 3: Conformations of surface ligands in atomistic and coarse-grained simulations. (a) Radial distribution functions of nitrogen in the charged amine groups relative to the center of the nanoparticle. (b)Radial distribution functions of nitrogen in the neutral amine groups relative to the center of the nanoparticle. (c) A snapshot from atomistic simulations that illustrates the two types of orientations of the neutral amine ligands, which extends to the solution and remains close to the nanoparticle surface,[15] respectively. (d) A snapshot from BMW-MARTINI simulations, the red sphere shows the position of a charged bead pointing into the solution, while the silver sphere shows an orientation of the neutral bead lying close to the particle surface. Results for the POL-MARTINI model are similar and thus not shown.

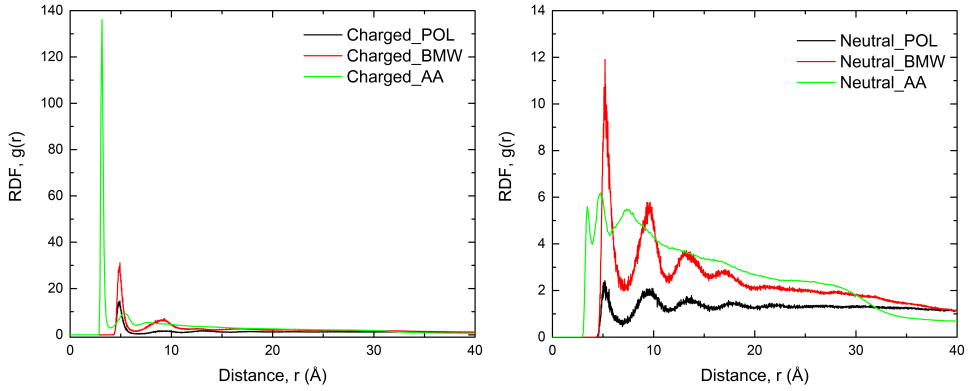

(a) (b)

Figure 4: Chloride Ion distribution around the nanoparticle in atomistic and coarse-grained simulations. (a) Radial distribution function of chloride ions around nitrogen in the charged amine groups; (b) Radial distribution function of chloride ions around nitrogen in the neutral amine groups.

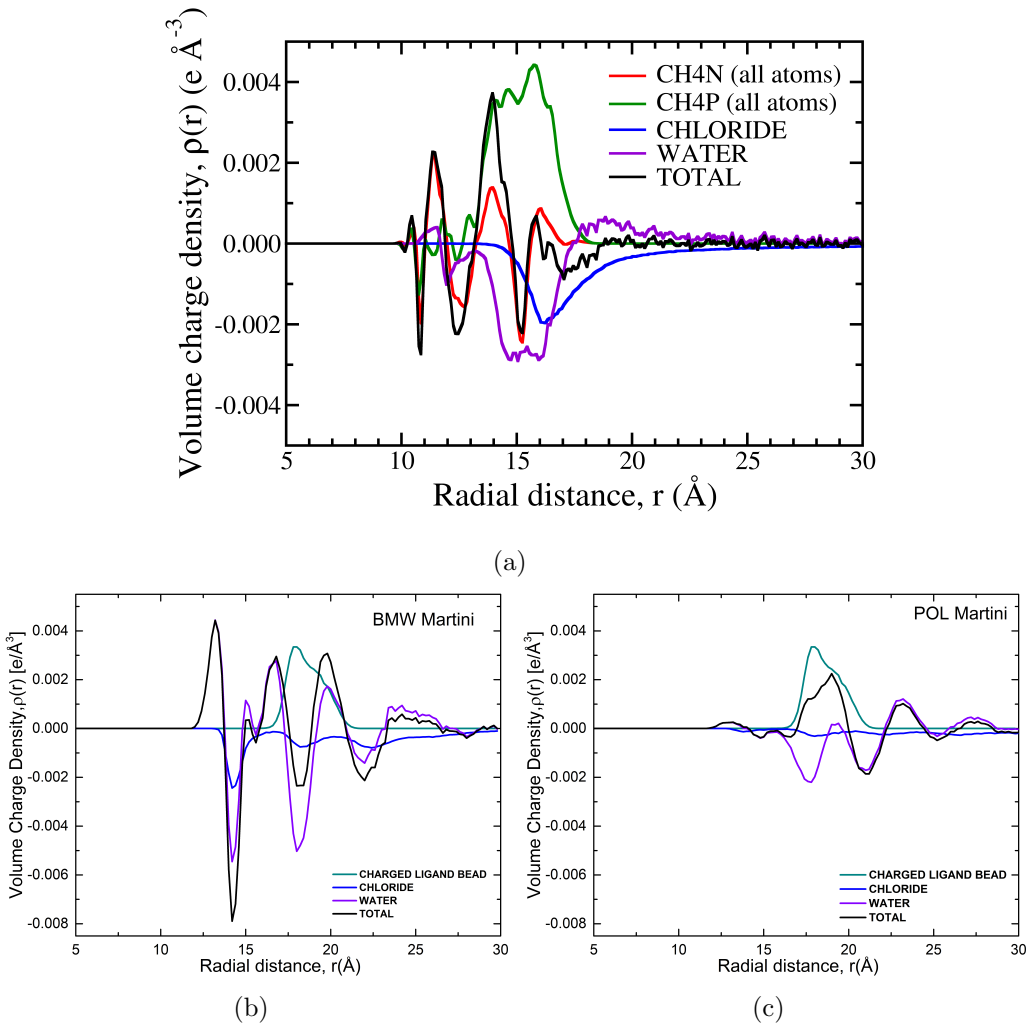

Figure 5: Total charge density and contributions from different components as functions of distance from the center of the nanoparticle. (a) atomistic simulation; (b) BMW- MARTINI; (c) POL-MARTINI. Note that the neutral amine ligand does not bear any partial charge and therefore does not contribute to the charge density plots in the MARTINI results.

3.2 Functionalized Nanoparticle with Lipid Bilayers

3.2.1 Binding to Lipid Bilayers

In atomistic simulations, the cationic nanoparticle does not exhibit any major attraction to a pure zwitterionic (DMPC) bilayer; by the end of $\sim$ 50 ns equilibrium simulation, as shown in Fig. 6a, the nanoparticle remains far from the bilayer. As discussed further below, previous atomistic simulations[11,61] of a similar (but not identical) cationic nanoparticle observed stable binding to a zwitterionic lipid bilayer after overcoming a small ($\sim$ 10 kJ/mol) barrier at room temperature. Therefore, we have conducted an independent MD simulation by first attching the nanoparticle on the surface of a DMPC bilayer with a weak harmonic restraint for $\sim$ 4 ns, after which the restraint is removed. As shown in Fig. 6c, the nanoparticle dissociates from the interface without exhibiting any obvious attraction; this observation is further supported by another independent simulation that employs a wall potential near the membrane/water interface (see **Supporting Information**). By contrast, the nanoparticle readily associates with the anionic bilayer that contains 9:1 DMPC:DMPG. As shown in Fig. 6d, the nanoparticle even penetrates into the anionic bilayer by a few Angstroms, leading to visible membrane deformation shown in Fig. 6b; the degree of deformation will be analyzed quantitatively below. Also visible from the snapshot shown in Fig. 6b is that the membrane bound nanoparticle leads to local clustering of anionic lipids (DMPG) in the upper leaflet, a phenomenon to be analyzed in detail below.

At the coarse-grained level, the encouraging result is that, with the BMW-MARTINI model, the nanoparticle quickly adsorbs to the anionic DMPC:DMPG membrane (Fig. 7a). As shown in Fig. 7b, the binding occurs quickly and the nanoparticle remains tightly associated with the membrane during the 1 μs simulation, despite a modest degree of fluctuation. The center of mass of the nanoparticle hovers between 20 Å to $\sim$6 Å from the phosphate plane (which is about 18 Å from the bilayer center), in comparison to the range of 18 Å to 11 Å observed in the atomistic simulations (Fig. 6d); i.e., the nanoparticle exhibits a similar

degree of shallow penetration into the bilayer (recall that the amine groups are ∼16-18 Å from the nanoparticle center, see Figs. 3). One difference visible from Fig. 7a is that, despite the binding of the nanoparticle, anionic lipid (DMPG) distribution in the upper leaflet does not appear to be significantly different from that in the lower leaflet; more quantitative analysis is given below.

Two other observations from the coarse-grained simulations, however, are less consistent with the atomistic simulations. First, in contrast to observation from the current atomistic simulations (see additional discussion in Sect.3.3), BMW-MARTINI simulation leads to rapid association of the cationic nanoparticle to the pure zwitterionic DMPC bilayer (Fig. 7c). As shown in Fig. 7d, the center of mass of the nanoparticle fluctuates between 21 Å and 10 Å from the phosphate plane during the 1 μs simulation, not too different from the behavior with a 9:1 DMPC:DMPG bilayer. In other words, the nanoparticle appears to be associated with DMPC in an equally stable fashion compared to the DMPC:DMPG bilayer. Evidently, electrostatics is not the only driving force at play for the nanoparticle-bilayer interaction with the BMW-MARTINI model. Second, with the POL-MARTINI model, the cationic nanoparticle does not exhibit any major association with either the zwitterionic DMPC or the anionic DMPC:DMPG bilayer. In Fig. 7e-f, results are shown explicitly for the situation with the DMPC:DMPG bilayer. The nanoparticle fluctuates wildly near the bilayer, sometime being more than 80 Å away from the phosphate plane. This is qualitatively consistent with the repulsive potential of mean force computed for a similar system using the POL-MARTINI model.[36] Therefore, the POL-MARTINI model appears to over-stabilize the cationic particle in the solution phase.

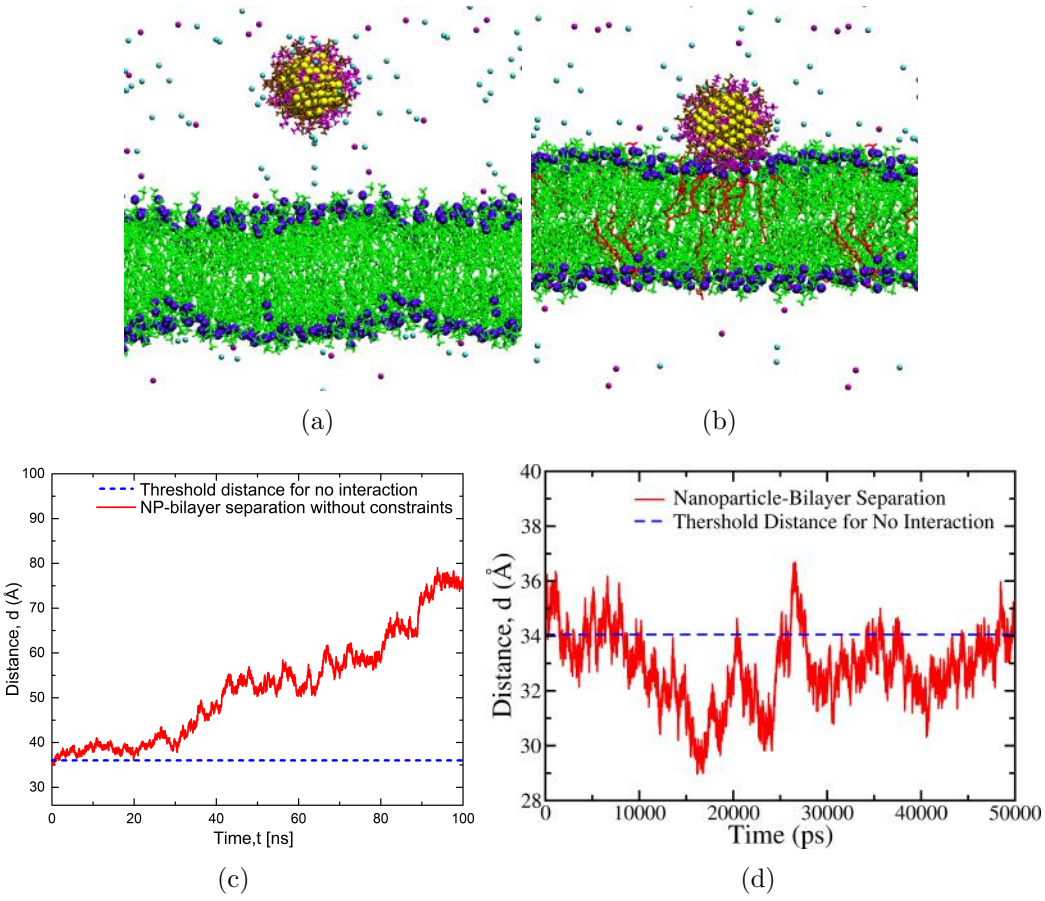

Figure 6: Behaviors of the nanoparticle at the membrane/water interface in atomistic simulations. (a-b) Snapshots at the end of the simulation for the case of zwitterionic (DMPC) and anionic (DMPC:DMPG) membrane, respectively. (c-d) Examples for the time dependence of the distance between the center of mass of the nanoparticle to the center of the lipid bilayer during (note that the phosphate plane is $\sim$ 18 Å from the bilayer center, and the ligands are $\sim$16-18 Å from the nanoparticle center, thus the threshold distance for no interaction is set approximately to 36 Å in the distance plots). For the DMPC:DMPG systems, approximately 450 ns of simulations in total have been conducted although only results for 50 ns are shown in panel d. For the DMPC system, in addition to an equilibrium simulation of 50 ns (the final snapshot is shown in panel a), a simulation is conducted where the nanoparticle is first harmonically restrained to the surface of the lipid bilayer for $\sim$ 4 ns, after which the restraint is removed; the time dependence of the nanoparticle-bilayer distance for the restraint-free part of the simulation is shown in panel c. Also see **Supporting Information** for an additional simulation in which the nanoparticle is subject to a wall potential near the bilayer interface.

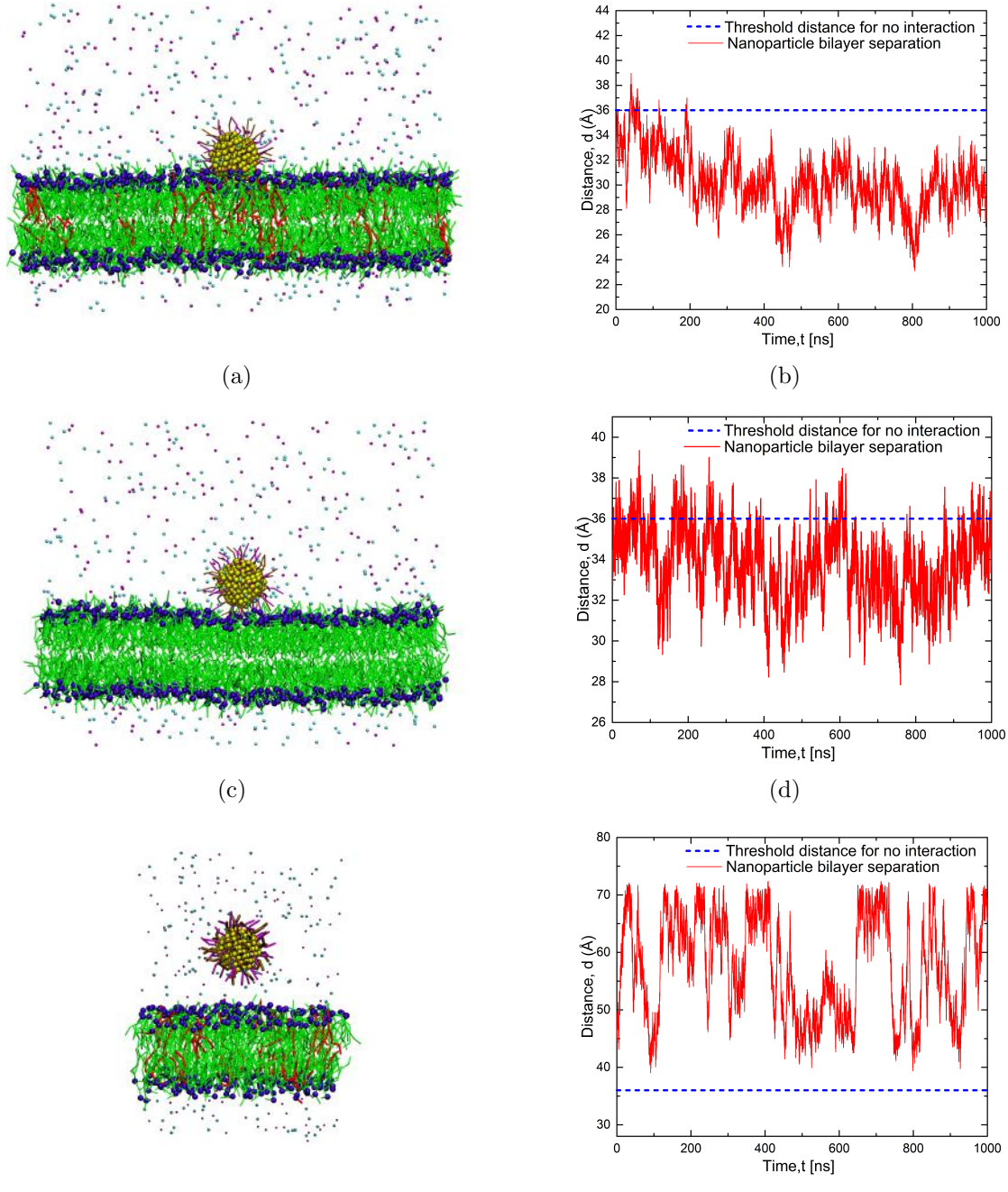

Figure 7: Same as Fig.6, but for various coarse-grained simulations. (a-b): BMW-MARTINI for the case of DMPC:DMPG membrane; (c-d): BMW-MARTINI for the case of DMPC membrane; (e-f): POL-MARTINI for the case of DMPC:DMPG membrane. For POL-MARTINI with DMPC membrane, the nanoparticle does not bind to the bilayer and therefore the results are not shown here.

3.2.2 Perturbation of Lipid Properties upon Nanoparticle Adsorption: Atomistic Simulations

As the cationic nanoparticle binds to the DMPC:DMPG bilayer, several lipid properties are clearly perturbed for the upper leaflet; we report these changes in this subsection. As already mentioned above, the snapshot from the atomistic simulation (Fig. 6b) clearly indicates that DMPG in the upper leaflet becomes clustered around the adsorbed nanoparticle. This is quantitatively reflected in the lateral radial distribution functions for the different lipid components in the bilayer; as shown in Fig. 8a, the DMPG:DMPG lateral distribution function in the upper leaflet is substantially elevated compared to either the DMPG:DMPG lateral distribution in the bottom leaflet or the DMPC:DMPC lateral distributions in either leaflet. The radial distribution functions of lipid phosphate group relative to the cationic amine groups in the nanoparticle (Fig. 8c) also clearly indicate that DMPG is preferentially clustered around the cationic amine groups relative to DMPC, as expected based on electrostatics.

The degree that DMPG properties are perturbed is further revealed by several other observables. As shown in Fig.9c-d, the segmental order parameters for the DMPC C2/C3 acyl chains (illustrated in Fig. 9a-b) hardly change at all upon nanoparticle binding, relative to a free DMPC:DMPG bilayer. By contrast, the order parameters for DMPG are perturbed for both the upper and lower leaflets upon nanoparticle binding, and the increase in the order parameters indicates more ordered lipid tails; the perturbation appears somewhat larger for the C3 chains (Fig. 9f) than for the C2 chains (Fig. 9e). Shown in Fig. S5 are the mean square displacements as functions of time for lipids in the upper and lower leaflets, again using a free 9:1 DMPC:DMPG bilayer as the reference. Evidently, the diffusion of DMPC is not much affected for either leaflet ($D_{PC} \sim 0.5/0.9 \times 10^{-7}$ cm^2/s for the upper/lower leaflets vs. $D_{PC} \sim 0.7 \times 10^{-7}$ cm^2/s for a free DMPC:DMPG bilayer), while the diffusion is considerably slower for the DMPG in the upper leaflet ($D_{PG} \sim 0.3 \times 10^{-7}$ cm^2/s vs. $D_{PG} \sim 1.1 \times 10^{-7}$ cm^2/s for a free DMPC:DMPG bilayer), due to the clustering of DMPG

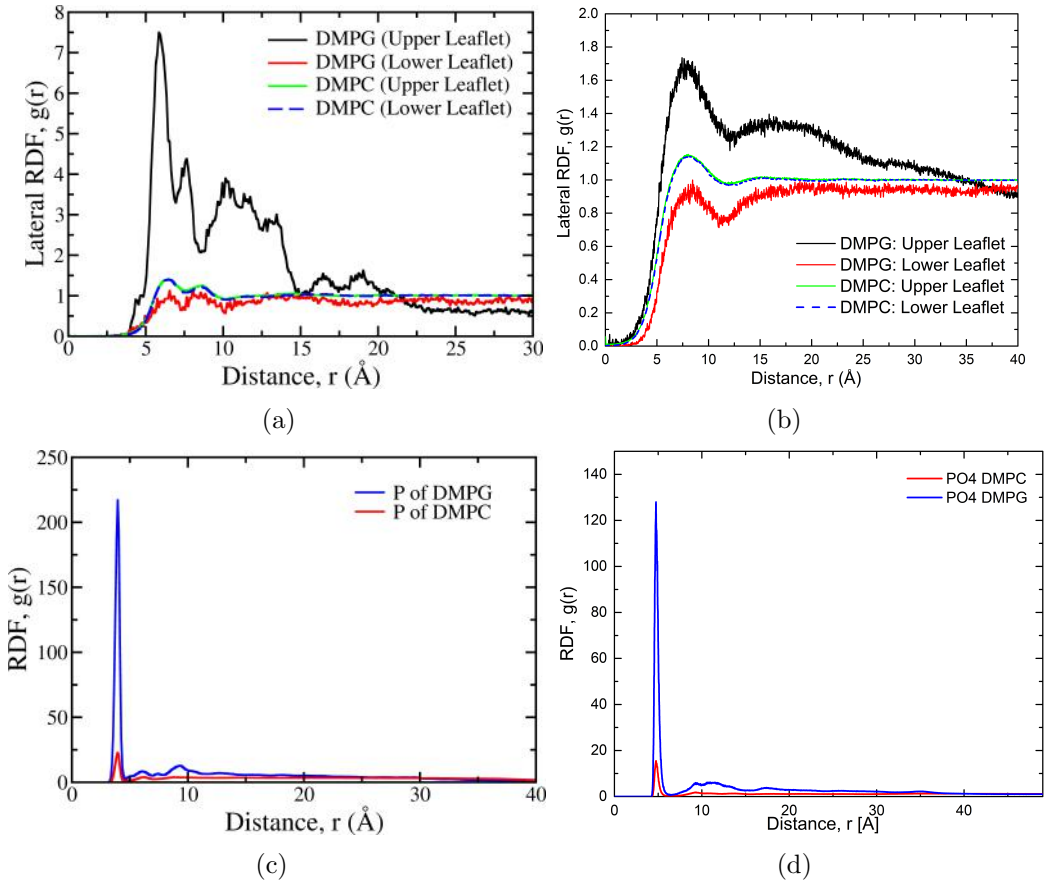

Figure 8: Lipid distributions in atomistic and BMW-MARTINI simulations of nanoparticle bound to the 9:1 DMPC:DMPG bilayer; the left column is atomistic while the right column is BMW-MARTINI. (a-b) Lateral radial distribution functions for the centers of mass of different lipid molecules; (c-d) Radial distribution functions for the phosphate group of lipids relative to the nitrogens in the charged amine groups; note that the concentrations for DMPC and DMPG differ by a factor of 9.

near the cationic nanoparticle. The diffusion of DMPG in the lower leaflet also appears to be perturbed slightly ($D_{PG} \sim 0.9 \times 10^{-7}$ cm^2/s), although the length of our simulation (~450 ns) is too short to allow a robust distinction relative to the case of a free DMPC:DMPG bilayer.

Also mentioned above is the observation that the nanoparticle penetrates shallowly into the bilayer, leading to local membrane thinning (the average phosphate-phosphate distance changes from 37.4 Å to 32.9 Å) and bending. The bending is quantified in Fig.10, in which the magnitude of curvature is evaluated by finite-difference of the Monge representation[62] of the

phosphate plane height function $h(x, y)$, following the protocol described in Ref.[36] The most significant curvature is observed at the site of nanoparticle adsorption and spans only a region comparable to the area per lipid molecule; therefore, the adsorption of a small nanoparticle studied here (diameter of 2 nm) has a rather local impact on the membrane structure. For the lower leaflet, the magnitude of curvature is very modest across the entire leaflet, indicating that the two leaflets are hardly coupled in terms of mechanical deformation, an assumption commonly made in continuum mechanics models for membrane deformation.[62,63]

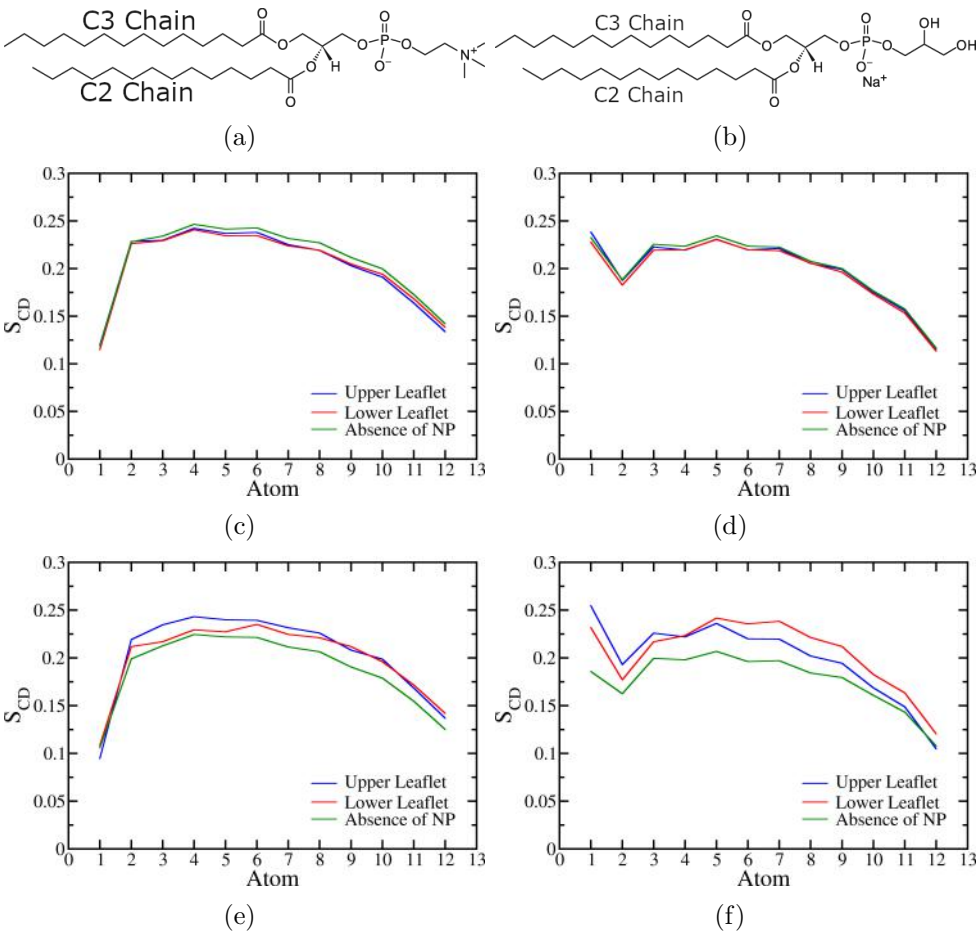

Figure 9: Lipid tail order parameters from atomistic simulations of nanoparticle bound to the 9:1 DMPC:DMPG bilayer. (a-b) Illustration of the C2 and C3 chains of DMPC and DMPG, respectively. (c-d) Segment order parameters for the C2 and C3 chains of DMPC lipids, respectively; for comparison, results for a free DMPC:DMPG bilayer in the absence of nanoparticle are also included. (e-f) Segment order parameters for the C2 and C3 chains of DMPG lipids, respectively; for comparison, results for a free DMPC:DMPG bilayer in the absence of nanoparticle are also included.

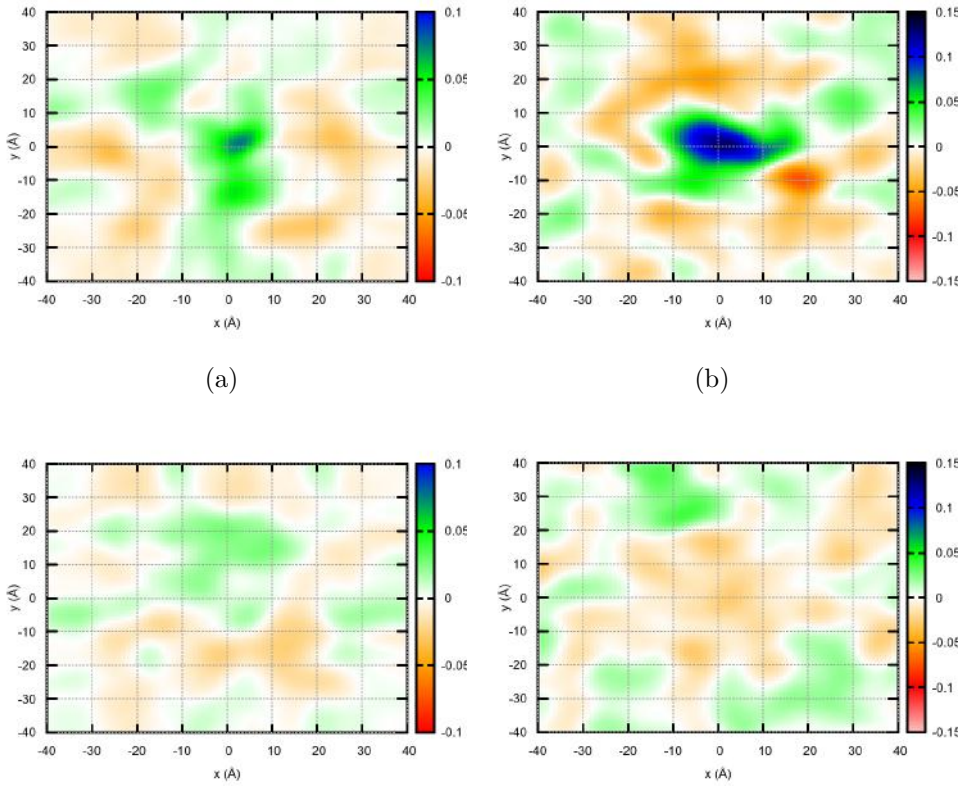

Figure 10: Total curvature of the (a-b) upper and (c-d) lower leaflets for the DMPC:DMPG bilayer upon nanoparticle adsorption from atomistic and coarse-grained (BMW-MARTINI) simulations; the left column is atomistic while the right column is BMW-MARTINI. The coordinates are re-centered at the site of nanoparticle adsorption (identified based on the nanoparticle center of mass) and averaged over 100 frames during the last 50 ns of the simulations.

3.2.3 Perturbation of Lipid Properties upon Nanoparticle Adsorption: Coarse-grained Simulations

At the coarse-grained level, only the BMW-MARTINI model leads to stable binding of the cationic nanoparticle on the DMPC:DMPG bilayer, thus the discussions below pertains to the BMW-MARTINI model only. As shown in the phosphate-amine radial distribution functions in Fig. 8d, the cationic particle does preferentially binds to DMPG over DMPC, qualitatively similar to the atomistic simulation results (Fig. 8c) although the degree of preference is much lower at the BMW-MARTINI level. This trend is also reflected in the lateral lipid distributions, which are quantitatively very different at the coarse-grained level as compared to the atomistic simulations. As shown in Fig. 8b, there is only minor difference between DMPG:DMPG and DMPC:DMPC lateral distributions at the coarse-grained level in either leaflet, in stark contrast to the atomistic results in Fig. 8a. The lack of strong DMPG clustering is consistent with the snapshot in Fig. 7a, which shows that DMPG distribution in the upper leaflet is not perturbed significantly even in the presence of the bound nanoparticle. This somewhat surprising observation can be explained by the finding here that with the BMW-MARTINI model, the cationic nanoparticle binds equally well with the DMPC bilayer; in other words, the nanoparticle does not exhibit a significantly stronger attraction with the anionic DMPG over DMPC (in comparison to atomistic descriptions), thus does not lead to significant clustering of DMPG.

The difference between the coarse-grained (BMW-MARTINI) and atomistic simulations is even more striking when the diffusion behaviors of lipids are examined. As shown in Fig. S6, with BMW-MARTINI, both DMPG and DMPC in the upper leaflet appear to diffuse *faster* in the presence of the nanoparticle, while the lower leaflet is hardly affected. Again, the results suggest that the cationic particle does not distinguish DMPC and DMPG with the BMW-MARTINI model.

For the membrane curvature and local thinning induced by the nanoparticle binding, the BMW-MARTINI results are largely consistent with the atomistic simulations (see Figs. 10).

Large curvature is generated only locally around the adsorption site of the nanoparticle, and the value of curvature is slightly higher at the coarse-grained level compared to atomistic result.

3.3 Discussion

By examining a fairly broad set of properties for a nanoparticle functionalized by alkyl amines in water and at the membrane/water interface, we are able to evaluate the performance of two popular coarse-grained models, POL-MARTINI and BMW-MARTINI using atomistic simulations with a non-polarizable empirical force field as reference. It is worth noting in this context that our recent analyses[15] of ligand conformation and nanoparticle electrostatic properties using models that explicitly included electronic polarization indicate that the current non-polarizable force field provides a reliable description for the surface properties of amine-functionalized gold nanoparticle. At the coarse-grained level, the surface properties of the amine-functionalized gold nanoparticle are generally in qualitative agreement with those from atomistic simulations, including the ligand orientations and interfacial charge density profile. On the other hand, due to the lower resolution of the amine group and salt ions, the range of charge oscillation is broader at the coarse-grained level. Between the two coarse-grained models analyzed here, BMW-MARTINI appears to give interfacial properties in closer agreement with the all-atom models, while POL-MARTINI underestimates the binding of Cl^- and water to the amine-functionalized cationic particle. These differences in the nanoparticle/water interfacial properties likely impact the interaction between the nanoparticle with other molecules, including lipid bilayers.

In terms of binding to lipid membrane, it is rather striking that both coarse-grained models tested here exhibit qualitative and quantitative differences from atomistic simulations. With POL-MARTINI, there is no affinity of the cationic nanoparticle to either zwitterionic (DMPC) or anionic (DMPC:DMPG) lipid bilayers, while both current and previous atomistic simulations[11,61] clearly indicate strong association of the nanoparticle to the anionic bilayer;

this observation is qualitatively consistent with the repulsive potential of mean force computed for a similar system in a recent study.[36] In addition to POL-MARTINI's inaccurate electrostatic potential profile at the membrane-water interface, as alluded to in several previous studies,[36,38,39] the less reliable charge density distribution at the particle/water interface observed in this study likely also contributes to the model's struggle with interfacial binding. In this context, while the weaker Cl^--amine interaction (especially with neutral amine) is noteworthy (Fig. 4b), the most significant difference between POL- and BMW-MARTINI again concerns the behavior of the water molecules at the interface.

With the BMW-MARTINI model, the cationic nanoparticle does bind to the anionic lipid bilayer with a similar degree of shallow penetration and fluctuation as observed in the atomistic simulation; the degree of local membrane bending induced by the nanoparticle binding is also comparable to atomistic results. These encouraging results are likely related to BMW-MARTINI's improved interfacial electrostatic potential, one of the properties that motivated the development of the model.[38,39] However, we note considerable discrepancies between BMW-MARTINI and current atomistic simulations regarding the impact of nanoparticle binding on lipid properties such as lateral distribution and diffusion constants. Regarding the latter, although it is well appreciated that it is generally more difficult to capture dynamic properties at the coarse-grained level,[13,64] it is remarkable that qualitatively different behaviors (e.g., slowing down vs. speeding up) are induced by the nanoparticle binding at the BMW-MARTINI and atomistic levels.

Another observation that warrants further discussion is that the BMW-MARTINI model leads to an equally strong association of the nanoparticle to the zwitterionic (DMPC) bilayer, in contrast to the current atomistic simulation, which indicates that the nanoparticle drifts away from the DMPC bilayer even if initially restrained to the interface for several nanoseconds (Fig. 6c). The latter observation appears to be at odds with recent studies of Akola and co-workers,[11,61] who observed that similar cationic gold nanoparticles bind to a zwitterionic lipid bilayer (POPC: 1-palmitoyl-2-oleoyl-*sn*-glycero-3-phosphocholine in Ref.[61] and DPSC:

di-stearoyl-phosphatidylcholine in Ref.[11]) once a small barrier ($\sim$ 10 kJ/mol) is overcome, as reflected by potential of mean force simulations. Such qualitative behavior appeared to be supported by temperature-dependent neutron reflectometry measurements,[11,65] which observed little change in the reflectivity profiles of the DSPC bilayer floating on a supported bilayer after introducing the cationic nanoparticle at room temperature; however, significant change in the reflectivity profiles was observed if the nanoparticles were introduced at the high temperature of 53 °C (which is still slightly below the gel-fluid phase transition temperature for DSPC, 55 °C), followed by the lowering of temperature back to 25 °C.

However, we note several differences between the current study and the work of Akola and co-workers. First, the gold nanoparticles studied in Refs.[11,65] were functionalized by quaternary amines with fairly long (8 CH_2 units) alkane chains; by contrast, we study primary amines with shorter (4 CH_2 units) alkane chains. Therefore, compared to our gold nanoparticles, those studied by Alkola and co-workers featured much larger hydrophobic components, which provided significant driving force for the nanoparticle to partition in the *hydrophobic tail region* of the lipid bilayer, as indicated by the deep well of the computed potential of mean force in the middle of the bilayer. Second, while our simulations employ all-atom force fields for both the nanoparticle and lipids (CHARMM36/INTERFACE force fields[45,47] for the ligands/lipids and gold atoms, respectively), the simulations in Refs.[11,61] employed an older united atom model for the lipid bilayer,[66] which is known to exhibit differences from all-atom models of lipids.[67] Therefore, to directly validate the atomistic simulation results for the nanoparticles studied here for zwitterionic bilayers, new experimental studies are needed. Along this line, we note that previous experimental studies did observe binding of primary amine functionalized gold nanoparticles to a supported zwitterionic (DOPC) bilayer,[40] although we caution that the binding was due at least in part to the negative surface potential generated by the anionic silica support.[68]

In the absence of experimental results for floating bilayers, considering the general success of the CHARMM36 force field model for lipid membrane properties and protein-membrane

interactions,[46,69] despite remaining challenges,[70] we suggest that the BMW-MARTINI model overestimates the affinity of the cationic nanoparticle to the zwitterionic (DMPC) bilayer; the lack of distinction between zwitterionic and anionic lipids in terms of their interactions with the cationic nanoparticle is also reflected by the generally similar behaviors of PC/PG lipids upon nanoparticle adsorption to the mixed PC:PG bilayer in BMW-MARTINI simulations, in contrast to observations in current atomistic simulations. Therefore, additional improvement of BMW-MARTINI is likely warranted to better distinguish zwitterionic and anionic lipids. Along this line, we note that the BMW-MARTINI model leads to considerably higher degree of water orientation at the nanoparticle/water interface than either POL-MARTINI or atomistic model as reflected by the interfacial charge distribution. As a result, overestimation of water mediated interaction observed in previous studies[71,72] for BMW-MARTINI might be partially responsible of the over-binding of the nanoparticle to the membrane surface, especially in the absence of an electrostatic driving force. We note that the general trends in the POL- and BMW-MARTINI simulations are not sensitive to the minor variations in the bead type of the amine group (see **Supporting Information**), which further supports the notation that the behavior is largely dictated by the description of interfacial water and ions at the coarse-grained level.

4 Concluding Remarks

Considering the complexity and involvement of multiple length scales of nano-bio interactions, coarse-grained models are expected to play an important role in exploring how nanoparticles interact with biological systems. The computational efficiency of coarse-grained models is highly beneficial to the sampling of a large number of system parameters, such as surface ligand composition and distribution, nanoparticle morphology and lipid membrane composition. Therefore, well calibrated coarse-grained models can be tremendously powerful at complementing experimental studies in terms of both mechanistic analysis and

design of novel nanoparticles.

On the other hand, the outcome of nano-bio interactions likely depends on the interplay of a rich set of competing interactions that involve not only the nanoparticles, surrounding biomolecules (e.g., proteins, lipids and carbonhydrates) but also small solutes (ions) and water molecules; some interactions (e.g., hydrophobic interactions) are primarily entropic rather than enthalpic in nature. Therefore, the demand on any computational model, either atomistic or coarse-grained, can be high even for qualitative predictions. Indeed, even for the question of whether a nanoparticle exhibits stable binding to the surface of a relatively simple lipid bilayer (either single-component or two-component), we observe different behaviors with atomistic (CHARMM36/INTERFACE) and two popular coarse-grained (POL- and BMW-MARTINI) models; for more detailed properties, such as lipid segregation and diffusion upon nanoparticle binding, there are more differences between coarse-grained and atomistic simulations. In fact, for the case of the zwitterionic bilayer, there appears to be qualitative discrepancy even between the current and previous atomistic simulations, although there are differences in the nanoparticle ligands that might be responsible for the observation. Therefore, validation and refinement of coarse-grained models with atomistic simulations *and* quantitative experimental data is indispensable for complex interfaces.

For the cationic particles analyzed here, the most striking differences among the coarse-grained and atomistic models involve the charge and water distributions at the particle/water interface, which are expected to contribute to the interaction between nanoparticles and other molecules through both enthalpic and entropic effects. While the BMW-MARTINI model exhibits overall closer agreement with atomistic simulations, further improvements are needed to better distinguish zwitterionic and anionic lipids in terms of their interactions with other molecules.

Acknowledgement

The work has been supported by the grant from the National Science Foundation CHE-1503408. Computational resources from the Extreme Science and Engineering Discovery Environment (XSEDE), which is supported by NSF grant number OCI-1053575, are greatly appreciated; computations are also supported in part by the Shared Computing Cluster, which is administered by Boston University's Research Computing Services. MD acknowledges Indo-U.S. Science and Technology Forum (IUSSTF) for a S. N. Bose Scholarship and the Department of Science and Technology (DST), Govt. of India for an INSPIRE Fellowship.

Supporting Information Available

Additional atomistic and coarse-grained simulation results that test the reproducibility of the observations are included. Mean square displacements of lipids from atomistic and coarse-grained simulations are also included. This material is available free of charge via the Internet at `http://pubs.acs.org/`.

References

(1) Verma, A.; Stellacci, F. Effect of Surface Properties on Nanoparticle-Cell Interactions. *Small* **2010**, *6*, 12–21.

(2) Albanese, A.; Tang, P. S.; Chan, W. C. W. The Effect of Nanoparticle Size, Shape, and Surface Chemistry on Biological Systems. *Annu. Rev. Biomed. Engn.* **2012**, *14*, 1–16.

(3) Nel, A. E.; Madler, L.; Velegol, D.; Xia, T.; Hoek, E. M. V.; Somasundaran, P.; Klaessig, F.; Castranova, V.; Thompson, M. Understanding Biophysicochemical Interactions at the Nano-bio Interface. *Nat. Mater.* **2009**, *8*, 543–557.

(4) Murphy, C. J.; Vartanian, A. M.; Geiger, F. M.; Hamers, R. J.; Pedersen, J.; Cui, Q.; Haynes, C. L.; Carlson, E. E.; Hernandez, R.; R. D. Klaper et al., Biological Responses to Engineered Nanomaterials: Needs for the Next Decade. *ACS Central Sci.* **2015**, *1*, 117–123.

(5) Wang, Y. L.; Cai, R.; Chen, C. Y. The Nano-Bio Interactions of Nanomedicines: Understanding the Biochemical Driving Forces and Redox Reactions. *Acc. Chem. Res.* **2019**, *52*, 1507–1518.

(6) Hochella Jr., M. F.; Mogk, D. W.; Ranville, J.; Allen, I. C.; Luther, G. W.; Matt, L. C.; McGrail, B. P.; Murayama, M.; Qafoku, N. P.; Rosso, K. M. et al., Natural, Incidental, and Engineered Nanomaterials and Their Impacts on the Earth System. *Science* **2019**, *363*, eaau8299.

(7) Troiano, J. M.; Kuech, T. R.; Vartanian, A. M.; Torelli, M. D.; Sen, A.; Jacob, L. M.; Hamers, R. J.; Murphy, C. J.; Pedersen, J. A.; Geiger, F. M. On Electronic and Charge Interference in Second Harmonic Generation Responses from Gold Metal Nanoparticles at Supported Lipid Bilayers. *J. Phys. Chem. C* **2016**, *120*, 20659–20667.

(8) Limo, M. J.; Sola-Rabada, A.; Boix, E.; Thota, V.; Westcott, Z. C.; Puddu, V.; Perry, C. C. Interactions between Metal Oxides and Biomolecules: from Fundamental Understanding to Applications. *Chem. Rev.* **2018**, *118*, 11118–11193.

(9) Riccardi, L.; Gabrielli, L.; Sun, X. H.; Biasi, F. D.; Rastrelli, F.; Mancin, F.; Vivo, M. D. Nanoparticle-Based Receptors Mimic Protein-Ligand Recognition. *Chem* **2017**, *3*, 92–109.

(10) Luo, Z.; Zhao, Y. F.; Darwish, T.; Wang, Y.; Hou, J.; Stellacci, F. Mass Spectrometry and Monte Carlo Method Mapping of Nanoparticle Ligand Shell Morphology. *Nat. Comm.* **2018**, *9*, 4478.

(11) Lolicato, F.; Joly, L.; Martinez-Seara, H.; Fragneto, G.; Scoppola, E.; Bombelli, F. B.; Vattulainen, I.; Akola, J.; Maccarini, M. The Role of Temperature and Lipid Charge on Intake/ Uptake of Cationic Gold Nanoparticles into Lipid Bilayers. *Small* **2019**, *15*, 1805046.

(12) Duan, G. X.; Kang, S. G.; Tian, X.; Garate, J. A.; Zhao, L.; Ge, C. C.; Zhou, R. H. Protein Corona Mitigates the Cytotoxicity of Graphene Oxide by Reducing Its Physical Interaction with Cell Membrane. *Nanoscale* **2015**, *7*, 15214–15224.

(13) Cui, Q.; Hernandez, R.; Mason, S.; Frauenheim, T.; Pedersen, J.; Geiger, F. M. Sustainable Nanotechnology: Opportunities and Challenges for Theoretical/Computational Studies. *J. Phys. Chem. B* **2016**, *120*, 7297–7306.

(14) Petertto, E.; Campomanes, P.; Stellacci, F.; Rothen-Rustishauser, B.; Petri-Fink, A.; Vanni, S. An Atomistic Look into Bio-inspired Nanoparticles and their Molecular Interactions with Cells. *Chimia* **2019**, *73*, 78–80.

(15) Liang, D. Y.; Hong, J. W.; Dong, F.; Bennett, J. W.; Mason, S. E.; Hamers, R. J.; Cui, Q. Analysis of Conformational Properties of Amine Ligands at the Gold/Water Interface with QM, MM and QM/MM simulations. *Phys. Chem. Chem. Phys.* **2018**, *20*, 3349–3362.

(16) Walsh, T. R. Pathways to Structure-Property Relationships of Peptide-Materials Interfaces: Challenges in Predicting Molecular Structures. *Acc. Chem. Res.* **2017**, *50*, 1617–1624.

(17) Heinz, H.; Ramezani-Dakhel, H. Simulations of Inorganic-bioorganic Interfaces to Discover New Materials: Insights, Comparisons to Experiment, Challenges, and Opportunities. *Chem. Soc. Rev.* **2016**, *45*, 412–448.

(18) Marrink, S. J.; Tieleman, D. P. Perspective on the Martini Model. *Chem. Soc. Rev.* **2013**, *42*, 6801–6822.

(19) Rossi, G.; Monticelli, L. Gold Nanoparticles in Model Biological Membranes: A Computational Perspective. *Biochim. Biophys. Acta* **2016**, *1858*, 2380–2389.

(20) Brancolini, G.; Tozzini, V. Multiscale Modeling of Proteins Interaction with Functionalized Nanoparticles. *Curr. Opin. Coll. Inter. Sci.* **2019**, *41*, 66–73.

(21) Van Lehn, R. C.; Ricci, M.; Silva, P. H. J.; Andreozzi, P.; Reguera, J.; Voitchovsky, K.; Stellacci, F.; Alexander-Katz, A. Lipid Tail Protrusions Mediate the Insertion of Nanoparticles into Model Cell Membranes. *Nat. Comm.* **2014**, *5*, 4482.

(22) Ding, H. M.; Ma, Y. Q. Theoretical and Computational Investigations of Nanoparticle-Biomembrane Interactions in Cellular Delivery. *Small* **2015**, *11*, 1055–1071.

(23) Alipour, E.; Halverson, D.; McWhirter, S.; Walker, G. C. Phospholipid Bilayers: Stability and Encapsulation of Nanoparticles. *Annu. Rev. Phys. Chem.* **2017**, *68*, 261–283.

(24) Zhang, S. L.; Gao, H. J.; Bao, G. Physical Principles of Nanoparticle Cellular Endocytosis. *ACS Nano* **2015**, *9*, 8655–8671.

(25) Spangler, E. J.; Upreti, S.; Laradji, M. Partial Wrapping and Spontaneous Endocytosis of Spherical Nanoparticles by Tensionless Lipid Membranes. *J. Chem. Phys.* **2016**, *144*, 044901.

(26) Bahrami, A. H.; Raatz, M.; Agudo-Canalejo, J.; Michel, R.; Curtis, E. M.; Hall, C. K.; Gradzielski, M.; Lipowsky, R.; Weikl, T. R. Wrapping of Nanoparticles by Membranes. *Adv. Coll. Inter. Sci.* **2014**, *208*, 214–224.

(27) Dasgupta, S.; Auth, T.; Gompper, G. Shape and Orientation Matter for the Cellular Uptake of Nonspherical Particles. *Nano Lett.* **2014**, *14*, 687–693.

(28) Bassereau, P.; Jin, R.; Baumgart, T.; Deserno, M.; Dimova, R.; Frolov, V. A.; Bashkirov, P. V.; Grubmuller, H.; Jahn, R.; Risselada, H. J. et al., The 2018 Biomembrane Curvature and Remodeling Roadmap. *J. Phys. D: Appl. Phys.* **2018**, *51*, 343001.

(29) Monopoli, M. P.; Aberg, C.; Salvati, A.; Dawson, K. A. Biomolecular Coronas Provide the Biological Identity of Nanosized Materials. *Nat. Nanotech.* **2012**, *7*, 779–786.

(30) Kinnear, C.; Moore, T. L.; Rodriguez-Lorenzo, L.; Rothen-Rustishauser, B.; Petri-Fink, A. Form Follows Function: Nanoparticle Shape and Its Implications for Nanomedicine. *Chem. Rev.* **2017**, *117*, 11476–11521.

(31) Ding, H.-M.; Ma, Y. Q. Computer Simulation of the Role of Protein Corona in Cellular Delivery of Nanoparticles. *Biomater.* **2014**, *35*, 8703–8710.

(32) Marrink, S. J.; Risselada, H. J.; Yefimov, S.; Tieleman, D. P.; de Vries, A. H. The MARTINI Force Field: Coarse Grained Model for Biomolecular Simulations. *J. Phys. Chem B* **2007**, *111*, 7812–7824.

(33) de Jong, D. H.; Singh, G.; Bennett, W. F. D.; Arnarez, C.; Wassenaar, T. A.; Schafer, L. V.; Periole, X.; Tieleman, D. P.; Marrink, S. J. Improved Parameters for the MARTINI Coarse-Grained Protein Force Field. *J. Chem. Theo. Comp.* **2013**, *9*, 687–697.

(34) Marrink, S. J.; Corradi, V.; Souza, P. C. T.; Ingolfsson, H. I.; Tieleman, D. P.; Sansom, M. S. P. Computational Modeling of Realistic Cell Membranes. *Chem. Rev.* **2019**, *119*, 6184–6226.

(35) Hong, J. W.; Hamers, R. J.; Pedersen, J. A.; Cui, Q. A Hybrid Molecular Dynamics/Multi Conformer Continuum Electrostatics (MD/MCCE) Approach for the Determination of Surface Charge of Nanomaterials. *J. Phys. Chem. C* **2017**, *121*, 3584–3596.

(36) Sheavly, J. K.; Pedersen, J. A.; Van Lehn, R. C. Curvature-driven Adsorption of Cationic Nanoparticles to Phase Boundaries in Multicomponent Lipid Bilayers. *Nanoscale* **2019**, *11*, 2767–2778.

(37) Yesylevskyy, S. O.; Schäfer, L. V.; Sengupta, D.; Marrink, S. J. Polarizable Water Model for the Coarse-Grained MARTINI Force Field. *PLoS Comput. Biol.* **2010**, *6*, e1000810.

(38) Wu, Z.; Cui, Q.; Yethiraj, A. A New Coarse-grained Model for Water: the Importance of Electrostatic Interactions. *J. Phys. Chem. B* **2010**, *114*, 10524–10529.

(39) Wu, Z.; Cui, Q.; Yethiraj, A. A New Coarse-grained Force Field for Membrane-peptide Simulations. *J. Chem. Theory Comput.* **2011**, *7*, 3793–3802.

(40) Melby, E. S.; Mensch, A. C.; Lohse, S. E.; Hu, D. H.; Orr, G.; Murphy, C. J.; Hamers, R. J.; Pedersen, J. A. Formation of Supported Lipid Bilayers Containing Phase-segregated Domains and Their Interaction with Gold Nanoparticles. *Environ. Sci. Nano* **2016**, *3*, 45–55.

(41) Cebecauer, M.; Amaro, M.; Jurkiewicz, P.; Sarmento, M. J.; Sachl, R.; Cwiklik, L.; Hof, M. Membrane Lipid Nanodomains. *Chem. Rev.* **2018**, *118*, 11259–11297.

(42) Jo, S.; Kim, T.; Iyer, V. G.; Im, W. CHARMM-GUI: A Web-based Graphical User Interface for CHARMM. *J. Comput. Chem.* **2008**, *29*, 1859–1865.

(43) Jo, S.; Lim, J. B.; Klauda, J. B.; Im, W. CHARMM-GUI Membrane Builder for Mixed Bilayers and Its Application to Yeast Membranes. *Biophys. J.* **2009**, *97*, 50–58.

(44) Phillips, J. C.; Braun, R.; Wang, W.; Gumbart, J.; Tajkhorshid, E.; Villa, E.; Chipot, C.; Skeel, R. D.; Kale, L.; Schulten, K. Scalable Molecular Dynamics with NAMD. *J. Comput. Chem.* **2005**, *26*, 1781–1802.

(45) Huang, J.; MacKerell, A. D. CHARMM36 All-atom Additive Protein Force Field: Validation Based on Comparison to NMR Data. *J. Comput. Chem.* **2013**, *34*, 2135–2145.

(46) Klauda, J. B.; Venable, R. M.; Freites, J. A.; O'Connor, J. W.; Tobias, D. J.; Mondragon-Ramirez, C.; Vorobyov, I.; MacKerell, A. D.; Pastor, R. W. Update of the

CHARMM All-atom Additive Force Field for Lipids: Validation on Six Lipid Types. *J. Phys. Chem. B* **2010**, *114*, 7830–7843.

(47) Heinz, H.; Lin, T. J.; Mishra, R. K.; Emami, F. S. Thermodynamically Consistent Force Fields for the Assembly of Inorganic, Organic, and Biological Nanostructures: The INTERFACE Force Field. *Langmuir* **2013**, *29*, 1754–1765.

(48) Jorgensen, W. L.; Chandrasekhar, J.; Madura, J. D.; Impey, R. W.; Klein, M. L. Comparison of Simple Potential Functions for Simulating Liquid Water. *J. Chem. Phys.* **1983**, *79*, 926–935.

(49) MacKerell, A. D.; Bashford, D.; Bellott, M.; Dunbrack, R. L.; Evanseck, J. D.; Field, M. J.; Fischer, S.; Gao, J.; Guo, H.; Ha, S. et al., All-Atom Empirical Potential for Molecular Modeling and Dynamics Studies of Proteins. *J. Phys. Chem. B* **1998**, *102*, 3586–3616.

(50) Nosé, S. A Unified Formulation of the Constant Temperature Molecular Dynamics Methods. *J. Chem. Phys.* **1984**, *81*, 511–519.

(51) Hoover, W. G. Canonical Dynamics: Equilibrium Phase-space Distributions. *Phys. Rev. A* **1985**, *31*, 1695–1697.

(52) Parrinello, M.; Rahman, A. Crystal Structure and Pair Potentials - A Molecular Dynamics Study. *Phys. Rev. Lett.* **1980**, *45*, 1196–1199.

(53) Ryckaert, J.-P.; Ciccotti, G.; Berendsen, H. J. C. Numerical Integration of the Cartesian Equations of Motion of a System with Constraints: Molecular Dynamics of n-alkanes. *J. Comput. Phys.* **1977**, *23*, 327–341.

(54) Darden, T.; York, D.; Pedersen, L. Particle Mesh Ewald: An N·logN method for Ewald sums in large systems. *J. Chem. Phys.* **1993**, *98*, 10089–10092.

(55) Steinbach, P. J.; Brooks, B. R. New Spherical-cutoff Methods for Long-range Forces in Macromolecular Simulation. *J. Comput. Chem.* **1994**, *15*, 667–683.

(56) Berendsen, H. J. C.; Postma, J. P. M.; van Gunsteren, W. F.; DiNola, A.; Haak, J. R. Molecular Dynamics with Coupling to an External Bath. *J. Chem. Phys.* **1984**, *81*, 3684.

(57) Hess, B.; Kutzner, C.; van der Spoel, D.; Lindahl, E. GROMACS 4: Algorithms for Highly Efficient, Load-Balanced, and Scalable Molecular Simulation. *J. Chem. Theory Comput.* **2008**, *4*, 435–447.

(58) Hu, H.; Yang, W. T. Free Energies of Chemical Reactions in Solution and in Enzymes with Ab Initio Quantum Mechanics/Molecular Mechanics Methods. *Annu. Rev. Phys. Chem.* **2008**, *59*, 573–601.

(59) Lu, X.; Fang, D.; Ito, S.; Okamoto, Y.; Ovchinnikov, V.; Cui, Q. QM/MM Free Energy Simulations: Recent Progress and Challenges. *Mol. Simul. (Special Issue on Free Energy Simulations)* **2016**, *42*, 1056–1078.

(60) Barrat, J.-L.; Hansen, J.-P. *Basic Concepts for Simple and Complex Liquids*; Cambridge University Press: Cambridge, UK, 2003.

(61) Martinez-Seara, E. H. H.; Gurtovenko, A. A.; Javanainen, M.; Häkkinen, H.; Vattulainen, I.; Akola, J. Cationic Au Nanoparticle Binding with Plasma Membrane-like Lipid Bilayers: Potential Mechanism for Spontaneous Permeation to Cells Revealed by Atomistic Simulations. *J. Phys. Chem. C* **2014**, *118*, 11131–11141.

(62) Boal, D. *Mechanics of the Cell*; Cambridge University Press: Cambridge, UK, 2002.

(63) Chernomordik, L. V.; Kozlov, M. M. Protein-lipid Interplay in Fusion and Fission of Biological Membranes. *Annu. Rev. Biochem.* **2003**, *72*, 175–207.

(64) Ayton, G. S.; Tepper, H. L.; Mirijanian, D. T.; Voth, G. A. A New Perspective on the Coarse-grained Dynamics of Fluids. *J. Chem. Phys.* **2004**, *120*, 4074–4088.

(65) Tatur, S.; Maccarini, M.; Barker, R.; Nelson, A.; Fragneto, G. Effect of Functionalized Gold Nanoparticles on Floating Lipid Bilayers. *Langmuir* **2013**, *29*, 6606–6614.

(66) Berger, O.; Edholm, O.; Jähnig, F. MolecularDynamics Simulations of a Fluid Bilayer of Dipalmitoylphosphatidylcholine at Full Hydration, Constant Pressure, and Constant Temperature. *Biophys. J.* **1997**, *72*, 2002–2013.

(67) Bennett, W. F. D.; Hong, C. K.; Wang, Y.; Tieleman, D. P. Antimicrobial Peptide Simulations and the Influence of Force Field on the Free Energy for Pore Formation in Lipid Bilayers. *J. Chem. Theory Comput.* **2016**, *12*, 4524–4533.

(68) Zimmermann, R.; K̈ttner, D.; Renner, L.; Kaufmann, M.; Zitzmann, J.; Müller, M.; Werner, C. Charging and Structure of Zwitterionic Supported Bilayer Lipid Membranes Studied by Streaming Current Measurements, Fluorescence Microscopy, and Attenuated Total Reflection Fourier Transform Infrared Spectroscopy. *Biointerphases* **2009**, *4*, 1–6.

(69) Pastor, R. W.; MacKerell, A. D. Development of the CHARMM Force Field for Lipids. *J. Phys. Chem. Lett.* **2011**, *2*, 1526–1532.

(70) Venable, R. M.; Krämer, A.; Pastor, R. W. Molecular Dynamics Simulations of Membrane Permeability. *Chem. Rev.* **2019**, *119*, 5954–5997.

(71) Wassenaar, T. A.; Ingolfsson, H. I.; Priess, M.; Marrink, S. J.; Schäfer, L. V. Mixing MARTINI: Electrostatic Coupling in Hybrid Atomistic-Coarse-Grained Biomolecular Simulations. *J. Phys. Chem. B* **2013**, *117*, 3516–3530.

(72) Choi, E.; Mondal, J.; Yethiraj, A. Coarse-Grained Models for Aqueous Polyethylene Glycol Solutions. *J. Phys. Chem. B* **2014**, *118*, 323–329.

TOC Graphics